

# Combined influence of oceanic and atmospheric circulations on Greenland Sea Ice concentration

Sourav Chatterjee<sup>1,2\*</sup>, Roshin P Raj<sup>3</sup>, Laurent Bertino<sup>3</sup>, Sebastian H. Mernild<sup>3</sup>, Subeesh MP<sup>1</sup>, Nuncio Murukesh<sup>1</sup>, Muthalagu Ravichandran<sup>1</sup>

<sup>1</sup>National Centre for Polar and Ocean Research, Ministry of Earth Sciences, India

<sup>2</sup>School of Earth, Ocean and Atmospheric Sciences, Goa University, India

<sup>3</sup>Nansen Environmental and Remote Sensing Center and Bjerknes Centre for Climate Research, Bergen, Norway

*Corresponds to:* Sourav Chatterjee (sourav@ncpor.res.in)

## **Abstract.**

The amount and spatial extent of Greenland Sea (GS) ice are primarily controlled by the sea ice export across the Fram Strait (FS) and by local seasonal sea ice formation, melting, and sea ice dynamics. In this study, using satellite passive microwave sea ice observations, atmospheric and a coupled ocean-sea ice reanalysis system, TOPAZ4, we show that both the atmospheric and oceanic circulation in the Nordic Seas (NS) act in tandem to explain the sea ice concentration (SIC) variability in the south-western GS. Northerly wind anomalies associated with anomalous low SLP over the NS reduce the sea ice export in the south-western GS due to westward Ekman drift of sea ice. On the other hand, the positive wind stress curl strengthens the cyclonic Greenland Sea Gyre (GSG) circulation in the central GS. An intensified GSG circulation may result in stronger Ekman divergence of surface cold and fresh waters away from the south-western GS. Both of these processes can reduce the freshwater content and weaken the upper ocean stratification in the south-western GS. At the same time, warm and saline Atlantic Water (AW) anomalies are recirculated from the FS region to south-western GS by a stronger GSG circulation. Under a weakly stratified condition, enhanced vertical mixing of these subsurface AW anomalies can warm the surface waters and inhibit new sea ice formation, further reducing the SIC in the south-western GS.

## **1 Introduction**

The freshwaters in the GS plays an important part for Nordic Seas overflow (Huang et al., 2020), which constitutes the lower limb of the Atlantic meridional overturning circulation (Chafik and Rossby 2019). The freshwater content in this region is largely driven by the amount of sea ice therein (Aagaard & Carmack 1989). Sea ice in GS is also important in determining shipping routes (Instanes et al. 2005; Johannessen et al. 2007), as well as to the regional marine ecosystem due to its impact on the light availability (Grebmeier et al. 1995). Most of the sea ice in the GS is exported from the central Arctic Ocean across the Fram Strait (FS) and is largely controlled by the ice-drift with the Transpolar Drift (Zamani et al. 2019).

32 Anomalous sea ice export through the FS is associated with events like the ‘Great Salinity Anomaly’ (Dickson et al. 1988)  
33 which can have impact on the freshwater content in the Nordic Seas. Therefore, it is quite evident that the changes in sea ice  
34 export through the FS influence the GS sea ice and thus the freshwater availability in the Nordic Seas (Belkin et al. 1998;  
35 Dickson et al. 1988; Serreze et al. 2006).

36 Even though it is one of the main mechanisms contributing to the overall SIC in GS, the relation between sea ice export  
37 through FS and SIC variability in GS is not very robust (Kern et al. 2010). This further points to the importance of local sea  
38 ice formation and sea ice dynamics in the GS. The impact of these processes can be realized prominently in the marginal ice  
39 zone (MIZ) in the south-western GS and in central GS (see Fig. 1 for approximate locations of the regions). These regions  
40 exhibit strong negative SIC trends during recent decades (Rogers and Hung, 2008, see also Fig. 1a in Selyuzhenok et al.  
41 2020). Changes in sea ice of this region can modify the deep water convection through influencing both the heat and salt  
42 budgets (Shuchman et al. 1998). Selyuzhenok et al. (2020) found that in spite of increasing sea ice export through the FS, the  
43 overall sea ice volume (SIV) in the GS has been decreasing during the period 1979–2016. They further attributed the  
44 interannual variability and decreasing trend of SIV to local oceanic processes, more precisely warmer AW temperatures in  
45 the Nordic Seas. Further local meteorological parameters e.g. air temperature, wind speed and direction along with oceanic  
46 waves, eddies have also been found to influence the sea ice properties in the central GS, particularly for the ‘Odden’ region  
47 (Campbell et al. 1987; Johannessen et al. 1987; Wadhams et al. 1996; Shuchman et al. 1998; Toudal 1999; Comiso et al.,  
48 2001).

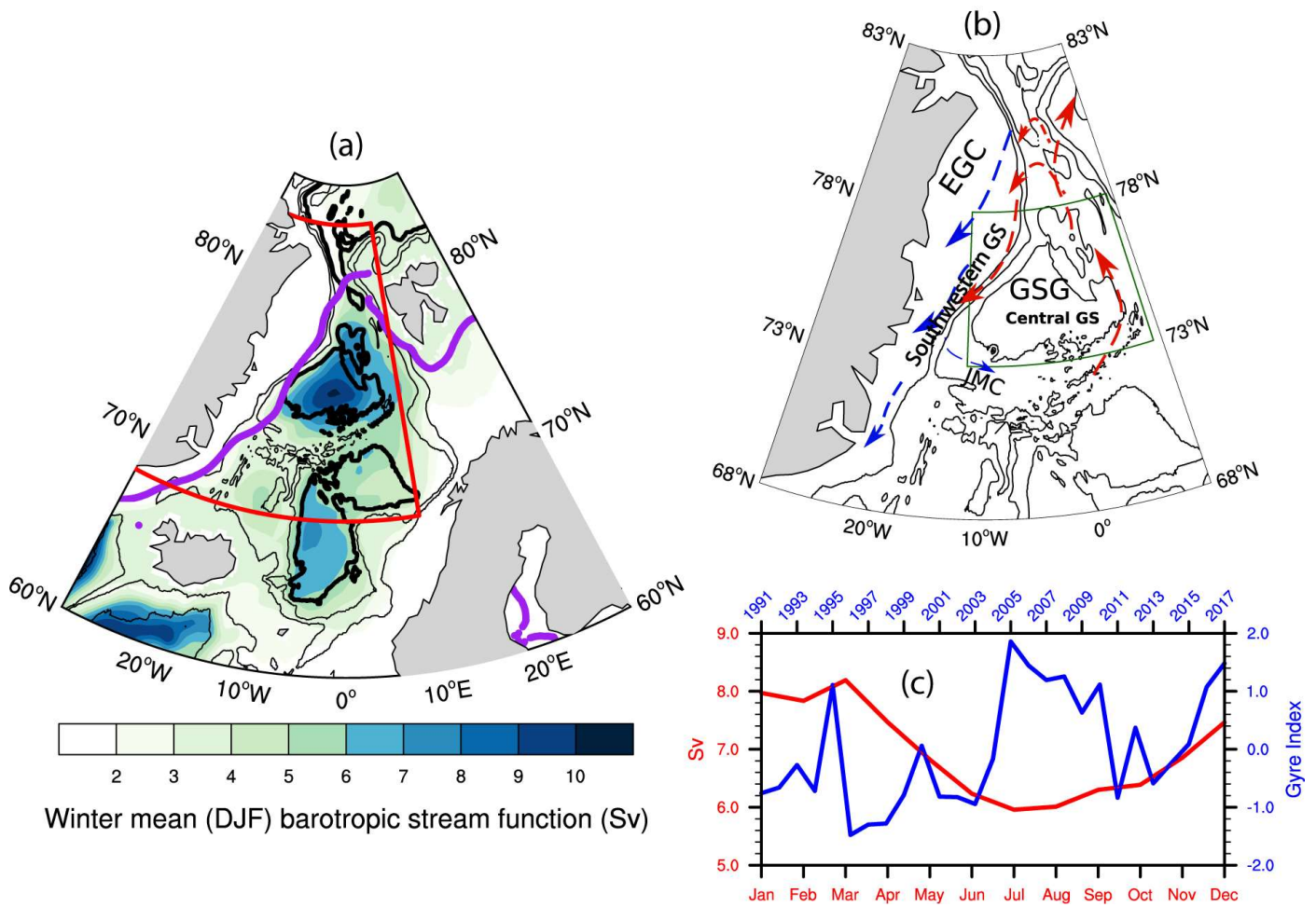
49 Besides the local factors, sea ice in the GS also responds to large-scale atmospheric forcing. For example, a high sea level  
50 pressure (SLP) anomaly over the NS results in anomalous southerly wind in the GS. The associated Ekman drift towards the  
51 central GS may assist the eastward expansion of the sea ice and SIC increase in the central GS (Germe et al. 2011).  
52 Selyuzhenok et al. (2020) also argued that consistent positive North Atlantic Oscillation (NAO) forcing in recent decades  
53 have led to warmer AW in the Nordic Seas and resulted in a declining sea ice volume trend. However, the response of  
54 Nordic Seas circulation to the atmospheric forcing and the mechanism through which it can influence the SIC in GS is not  
55 studied in detail.

56  
57 The Greenland Sea Gyre (GSG) is a prominent large-scale feature of the Nordic Seas circulation and can be identified as a  
58 cyclonic circulation in the central GS basin (Fig. 1). It is known to respond to the atmospheric forcing in the NS and  
59 contribute to AW heat distribution in the Nordic Seas (Hatterman et al. 2016; Chatterjee et al. 2018). A stronger GSG  
60 circulation increases the AW temperature in the FS by modifying the northward AW transport in its eastern side (Chatterjee  
61 et al. 2018). A simultaneous increase in its southward flowing western branch, constituting the southern recirculation  
62 pathway of AW (Hattermann et al. 2016; Jeansson et al. 2017), can increase the heat content in the south-western GS  
63 through a stronger and warmer recirculation of AW (Chatterjee et al. 2018). The return AW, even after significant  
64 modification, remains denser than the local cold and fresh surface waters and thus mostly remain in the subsurface

65 (Schlichtholz & Houssais 1999; Eldevik et al. 2009). However, enhanced vertical winter mixing can cause warming of the  
66 surface waters in the GS (Våge et al., 2018). Further, the eastward flowing Jan Mayen Current (JMC), originated from the  
67 East Greenland Current (EGC), constitutes the south-western closing branch of the cyclonic GSG circulation in the GS (Fig.  
68 1b). The east-ward extension of the cold and fresh JMC into the central GS basin helps in both new sea ice formation and  
69 advection of sea ice from the EGC (Wadhams & Comiso 1999). Changes in GSG circulation and associated AW  
70 recirculation in GS may also influence the JMC strength and temperature. Thus given the potential role of GSG in modifying  
71 the oceanic conditions, it is important to understand how the response of GSG circulation to the atmospheric forcing can  
72 influence the SIC in the GS.

73

74 In this study we hypothesize that the interannual winter mean SIC variability in GS can be explained by the combined  
75 influence of atmospheric and oceanic circulations, more precisely the GSG circulation. Using a combination of satellite  
76 passive microwave SIC, a coupled sea ice ocean reanalysis and atmospheric reanalysis data, we show that changes in the  
77 GSG dynamics and resulting AW transport in GS can potentially influence the SIC in the south-western GS. Further, we also  
78 show that the atmospheric circulation associated with the GSG circulation variability provides the favourable conditions for  
79 the GSG's control on the SIC variability in the south-western GS region. Section 2 describes the data and methods applied in  
80 the study following the results in section 3. Discussions and conclusions are mentioned in section 4.



81  
 82 **Figure 1:** a) Winter mean (DJF) barotropic stream function for the period 1991–2017. The region marked in red indicates  
 83 the Nordic Seas region. The purple line shows the mean DJF sea ice extent for the study period. b) Schematic of the major  
 84 currents and discussed in the text. JMC: Jan Mayen Current; EGC: East Greenland Current; GSG: Greenland Sea Gyre.  
 85 Warm currents are drawn in red and cold currents are in blue. Black contours are showing bottom topography drawn at every  
 86 1000 m. The thick black contour indicates the 3000m isobath. The marked region in dark green is used to calculate the ‘gyre  
 87 index’ as detailed in the next section. c) The blue line indicates the gyre index used in this study and the red line shows the  
 88 annual cycle of the strength of GSG circulation determined by averaging barotropic stream function within the 3000m  
 89 isobath in the region marked in (b).

## 90 **2. Data**

### 91 **2.1 Atmospheric data:**

92 Monthly mean sea level pressure (SLP) data was obtained from the ERA Interim reanalysis (Dee et al. 2011) for the period  
93 1991–2017 on a 0.5 by 0.5 degree grid resolution. Monthly anomalies were calculated from the monthly climatology field  
94 using the full time period (1991–2017) and were averaged for December-January-February (DJF). For the linear regression  
95 analysis the DJF averaged SLP anomalies were detrended.

96

### 97 **2.2 Oceanic data:**

98 Monthly mean oceanic data used in this study were taken from TOPAZ4, a coupled ocean and sea ice data assimilation  
99 system for the North Atlantic and the Arctic. TOPAZ4 is based on the Hybrid Coordinate Ocean Model (HYCOM, with 28  
100 hybrid z-isopycnal layers at a horizontal resolution of 12 to 16 km in the Nordic Seas and the Arctic) and Ensemble Kalman  
101 Filter data assimilation, the results of which have been evaluated in earlier studies (Lien et al. 2016; Xie et al. 2017;  
102 Chatterjee et al. 2018; Raj et al. 2019). TOPAZ4 represents the Arctic component of the Copernicus Marine Environment  
103 Monitoring Service (CMEMS) and is forced by ERA Interim reanalysis and assimilates (every week) observations from  
104 different platforms. The detailed setup and performance of the TOPAZ4 reanalysis, including the counts of observations and  
105 the temporal variations of the data counts are described in Xie et al. (2017). Of particular relevance for GS are the  
106 assimilation of Argo profiles, research cruises CTDs from Institute of Oceanology Polish Academy of Science (IOPAS) and  
107 Alfred-Wegener Institute (AWI) (Sakov et al. 2012), satellite sea ice concentration, sea surface temperature and sea level  
108 anomaly from the CMEMS platforms.

109

### 110 **2.3 Sea ice data:**

111 Monthly mean sea ice concentrations (SIC) from Nimbus-7 SMMR and DMSP SSM/I-SSMIS Passive Microwave Data,  
112 Version 1 (Cavalieri et al. 1996) were obtained from the National Snow and Ice Data Centre for the period 1991–2017. The  
113 dataset provides a continuous time series of SIC on a polar projection at a grid scale size of 25km by 25km. Sea ice velocity  
114 data was taken from the Polar Pathfinder Daily 25 km EASE-Grid Sea Ice Motion Vectors (Tschudi et al. 2019).

115

### 116 **2.4 Methods and Evaluation of TOPAZ4**

117 We estimated the strength of the GSG circulation by area-averaging the winter-mean (DJF) barotropic stream function  
118 anomalies within the 3000m isobath in the region 73 N:78 N; 12 W:9 E (as marked with green box in Fig. 1b). The area-  
119 averaged values were then standardized over the complete time period 1991–2017 to estimate the ‘gyre index’ (Fig. 1c). In  
120 this study we focused only on the winter (DJF) season as the local sea ice in GS can only form during winter and also the  
121 strength of the GSG circulation peaks during winter (Fig. 1c). Composite analysis of DJF mean potential temperature  
122 anomaly was performed by averaging the same for strong and weak gyre index years which were determined when the gyre

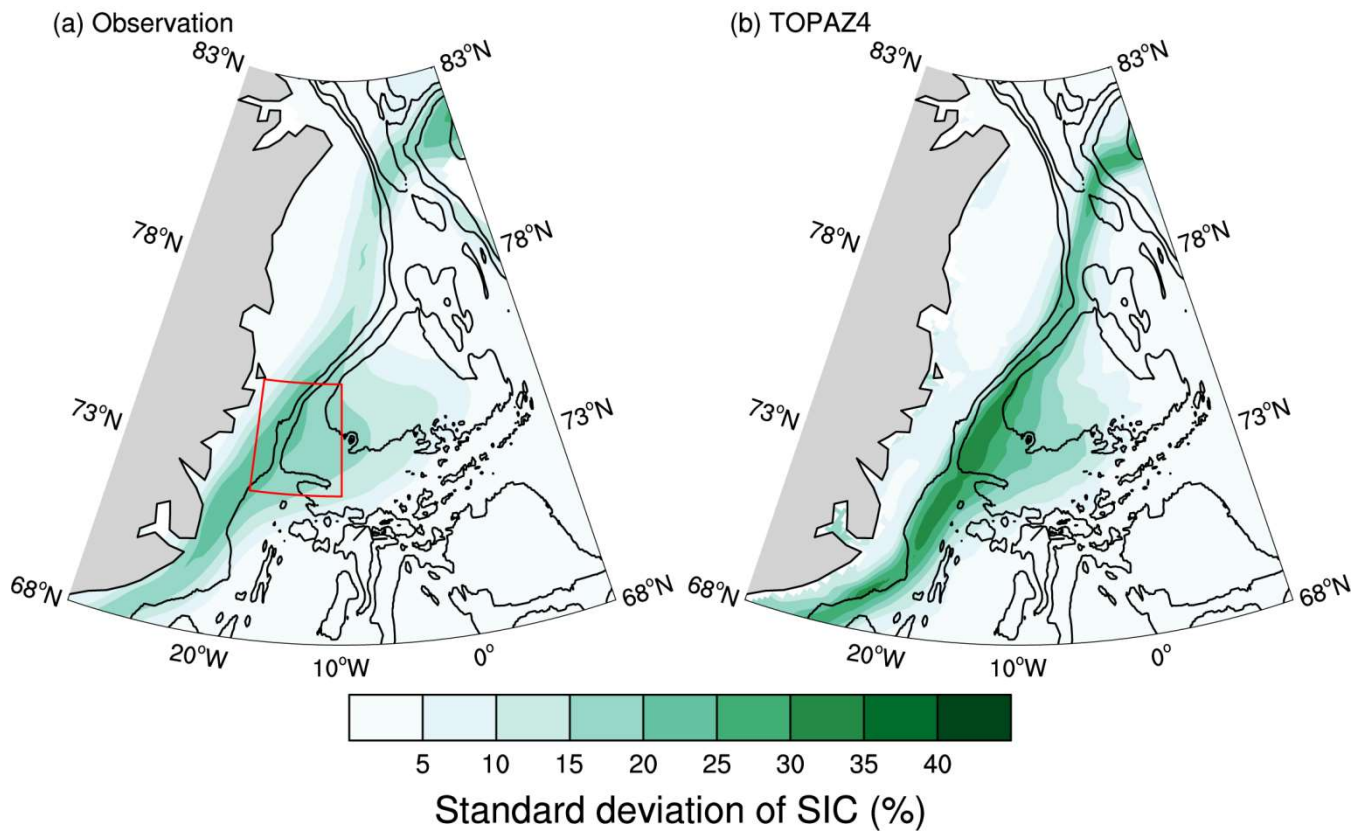
123 index crosses the 0.75 and -0.75 mark respectively. The 0.75 threshold was chosen to consider only the sufficiently  
124 strong/weak gyre circulation periods. Throughout the article, all regression and correlation analysis were performed with the  
125 detrended time series for the corresponding variables. Freshwater content was calculated using the following formula

$$\int_z^{surf} \frac{S_{ref} - S}{S_{ref}} dz$$

126 where,  $S$  is salinity and the reference salinity  $S_{ref}$  is chosen as 34.8 psu.

127

128 The standard deviation of winter-mean DJF SIC, in both observation and TOPAZ4, showed high variability along the MIZ in  
129 south-western GS and the Odden region in central GS (Fig. 2). Note that, the TOPAZ4 reanalysis data exhibits a more  
130 confined MIZ than observations, which is a known model deficiency (Sakov et al. 2012). The sea ice model (Hunke and  
131 Dukowicz, 1997), used in TOPAZ4, has a narrower transition zone between the pack ice and the open ocean. Although  
132 assimilation of the sea ice observations does slightly improve the position of MIZ in TOPAZ4 compared to observation, the  
133 sharp transition in a narrow band still remains, which could have resulted in higher standard deviations in a narrow MIZ of  
134 TOPAZ4 as observed in Fig. 2b. However, as we will find in the next section, the sea ice response to the atmospheric and  
135 oceanic processes explained in the study can be significantly found in both the observation and TOPAZ4 with slightly higher  
136 signals along the MIZ in TOPAZ4. Thus the higher signal-to-noise ratio in TOPAZ4 should not affect the qualitative aspects  
137 of the processes and their influence on SIC, which is the main objective of the study.



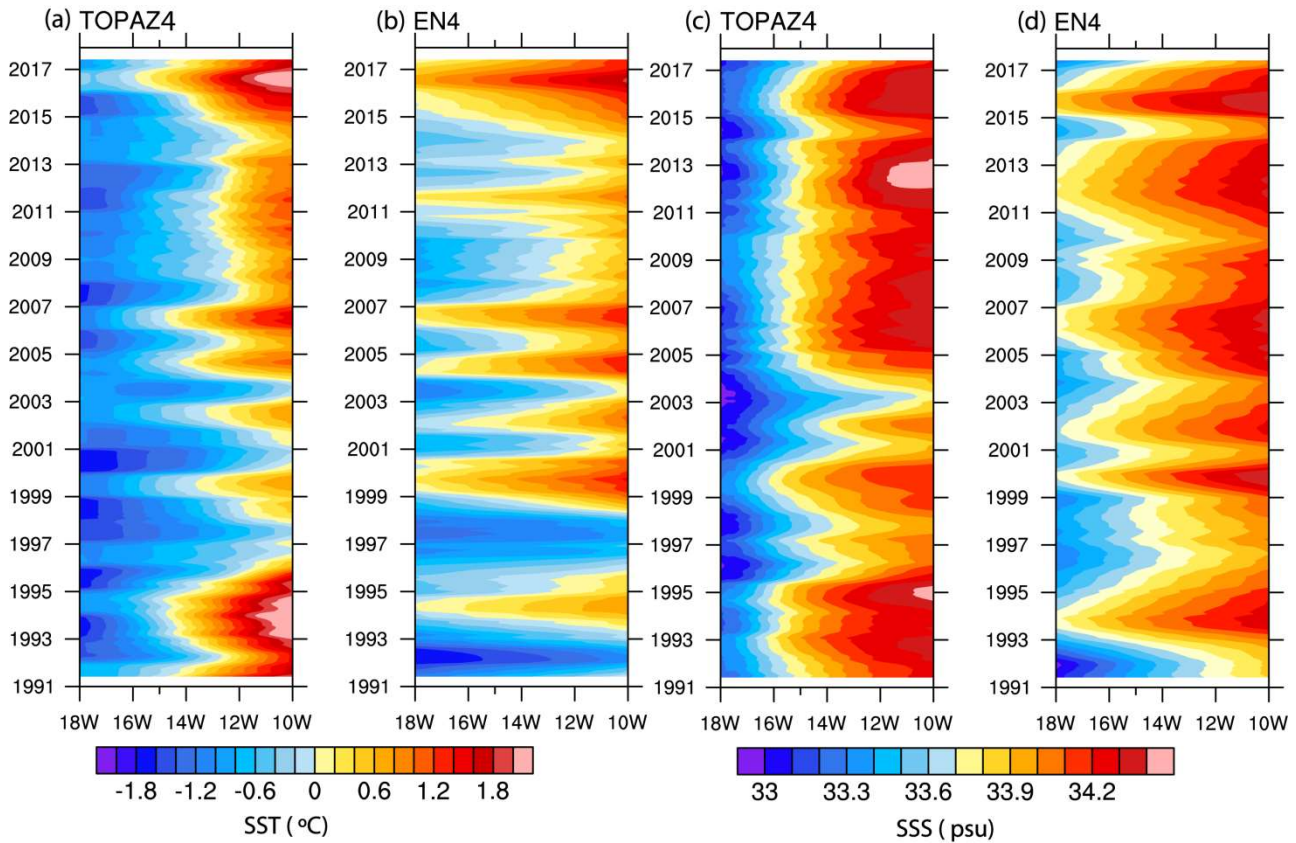
138

139

140 **Figure 2:** Standard deviations of DJF mean sea ice concentration for the period 1991–2017 from (a) satellite observations  
 141 (b) TOPAZ4 reanalysis. The red box with high values is drawn over the region 72N:75N; 18W:10W and is referred to as  
 142 south-western GS hereafter.

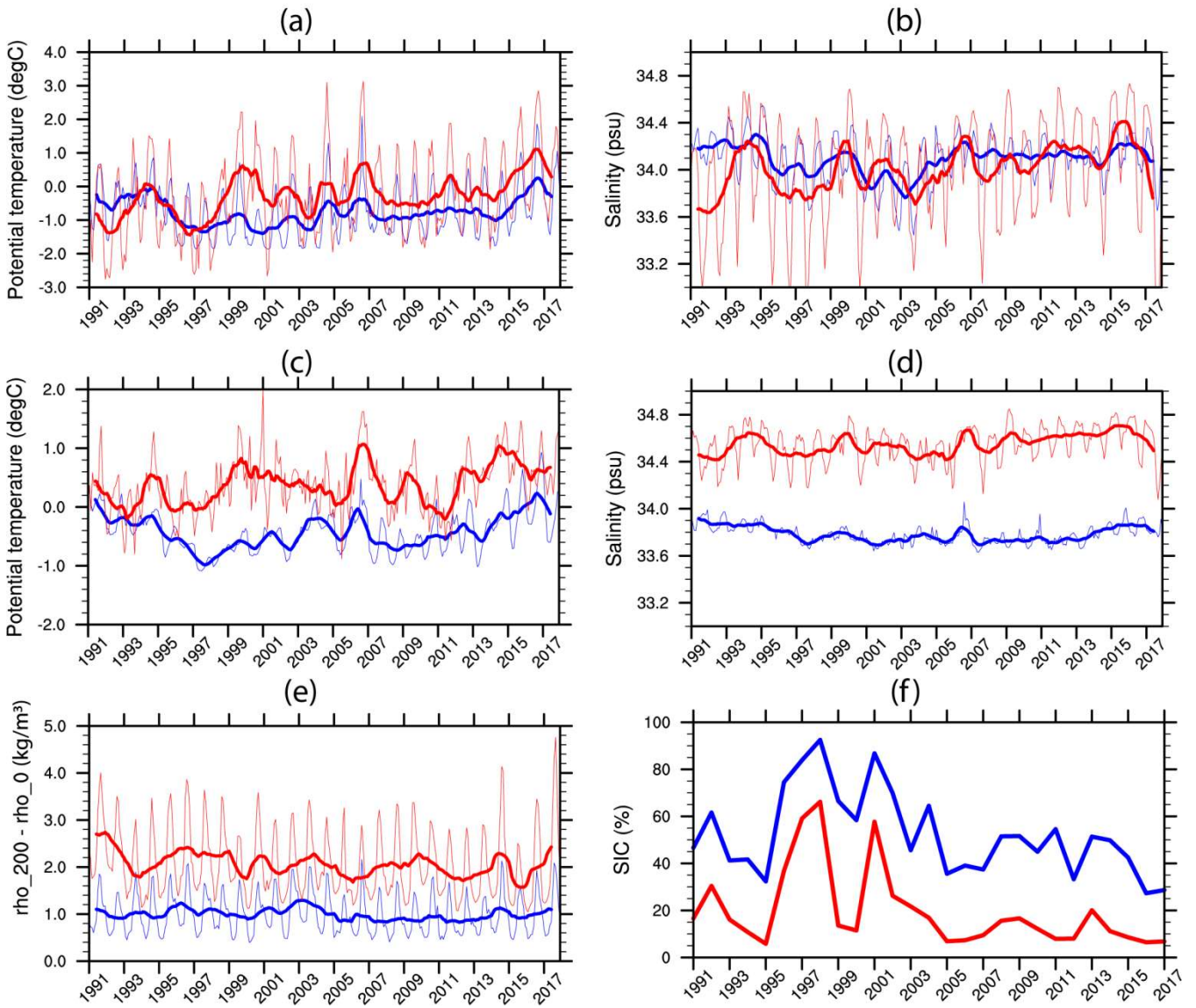
143 For evaluation of the oceanic conditions in TOPAZ4 we used temperature and salinity observations obtained from EN4  
 144 (version 4.2.1) quality controlled analyses with Levitus et al. (2009) corrections applied. Here we chose to compare the  
 145 oceanic parameters in a region (as marked in Fig. 2) in south-western GS where the standard deviation of the SIC is found to  
 146 be maximum both in TOPAZ4 and observations. Also we will show in the next section that SIC response to the processes  
 147 described here is most profound in this region. Hereafter we refer to this region as south-western GS for simplicity. Fig. 3  
 148 shows the spatio-temporal patterns of sea surface temperature (SST) and salinity (SSS) in south-western GS as found in  
 149 TOPAZ4 and EN4. Although the temporal evolution of these parameters are well captured in TOPAZ4, compared to  
 150 observation, the westward extension of the warm and saline waters was found to be less in TOPAZ4. This indicates that the  
 151 front between the cold and fresh waters along the Greenland shelf and the warm and saline waters in the south-western GS is  
 152 slightly shifted towards the east in TOPAZ4 compared to observation. This could be a reason for the fact that higher standard

153 deviation of SIC is found slightly toward the east in TOPAZ4 than observations (Fig. 2). In south-western GS, both the  
 154 surface and subsurface temperature in TOPAZ4 was found to be colder compared to observations (Fig. 4). The negative  
 155 biases in TOPAZ4 were more profound in the subsurface for both temperature and salinity. Xie et al., (2017) also found a  
 156 similar result with TOPAZ4 and attributed it to sparse observations. Using the potential density difference between 200m  
 157 and the surface as an indicator of the stratification, we found that TOPAZ4 has weaker stratification compared to  
 158 observations (Fig. 4e). Consistent with the cold bias in TOPAZ4, winter-mean SIC in TOPAZ4 is higher than the satellite  
 159 observation in the south-western GS (Fig. 4f). However, we found a strong correlation ( $r=0.9$ ) between the SIC in  
 160 observation and TOPAZ4. This indicates that the interannual variability of SIC, which is the focus of the study, is quite  
 161 consistent in both TOPAZ4 and observation.



162

163 **Figure 3:** Hovmöller (longitude-time) diagram of the monthly SST (°C; a,b) and SSS (psu; c,d) over the region over 72 N:75  
 164 N; 18 W:10 W in the south-western GS as marked in Fig. 2. (a) and (c) are for TOPAZ4 and (b) and (d) for EN4  
 165 observations. In all cases data were smoothed with one year running mean.



167

168

169

170

171

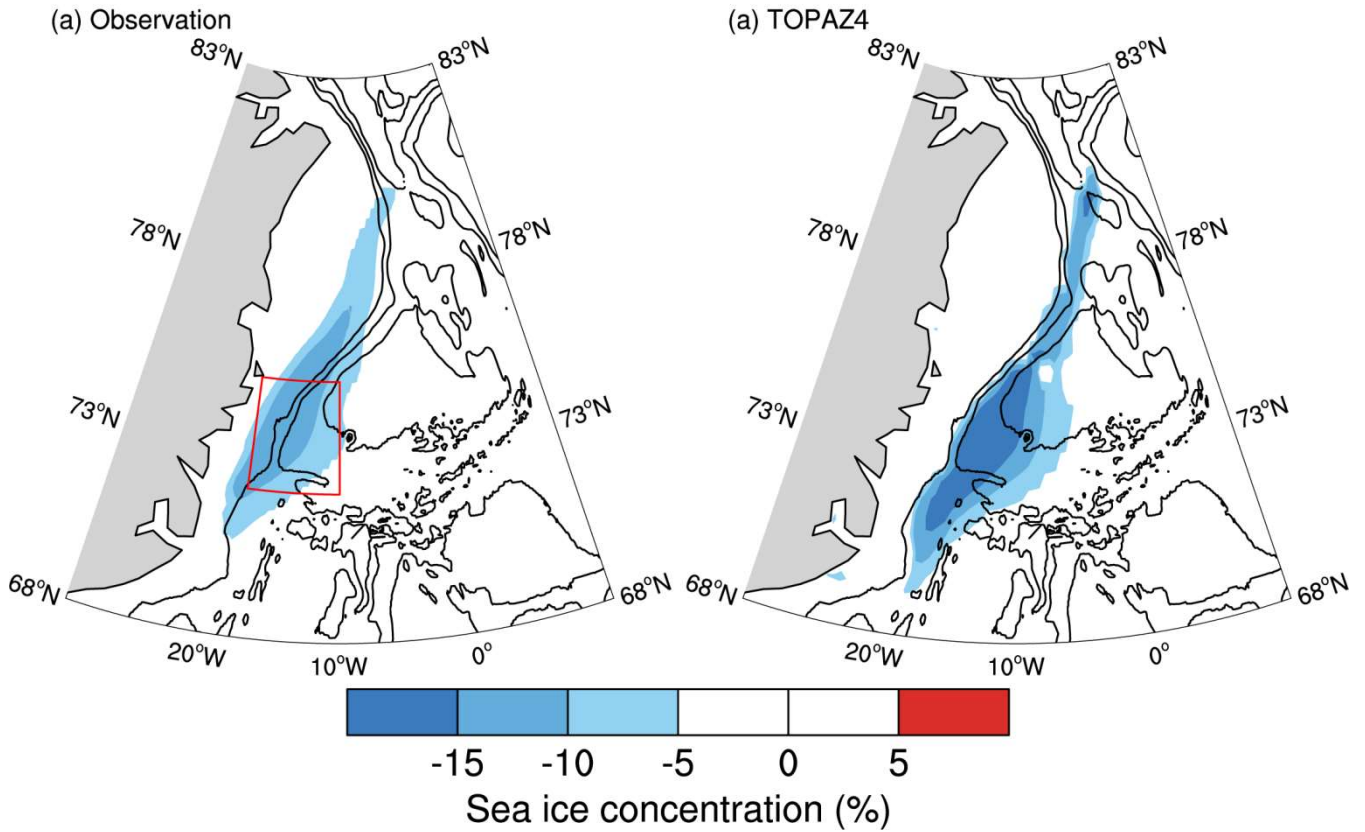
172

173

**Figure 4:** Comparison between EN4 observation (red lines) and TOPAZ4 (blue lines). Monthly mean (thin lines) and one year running mean (thick lines) of potential temperature (a,c), salinity (b,d) and stratification index (e, difference of potential density between 200m and surface) averaged over 72 N:75 N; 18 W:10 W in the south-western GS as marked in Fig. 2. (a,b) are for 0-50m depth average and (c,d) for 100-400m depth average. (f) DJF mean sea ice concentration in the same region from satellite observation (red) and TOPAZ4 (blue).

175 **3. Results**

176 The regression map of winter mean SIC on the gyre index showed significant negative SIC in the south-western GS (Fig. 5).  
 177 The spatial pattern of the regression coefficients closely resembles the standard deviation of winter mean SIC in the GS, as  
 178 shown in Fig. 2. This indicates that a considerable amount of the SIC variability in GS can be associated with GSG  
 179 circulation. However, it should be noted that the atmospheric forcing in the NS can influence both the GSG circulation  
 180 (Aagaard 1970; Legutke 2002; Chatterjee et al. 2018) and SIC variability in the GS (Germe et al. 2011).



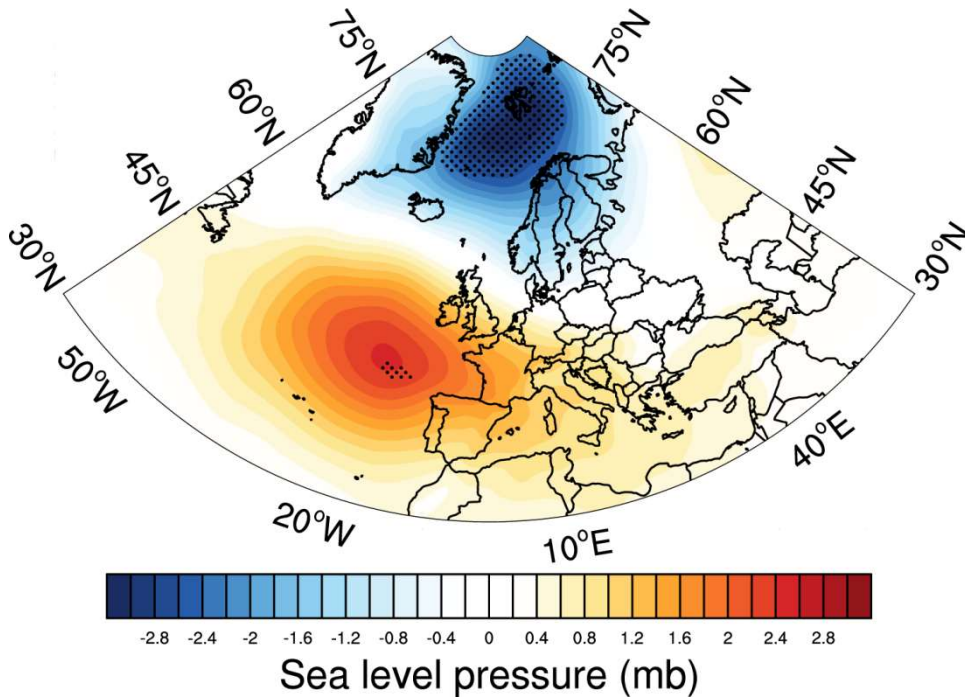
181

182

183

184 **Figure 5:** Linear regression of winter mean (DJF) sea ice concentration from (a) satellite observation (b) TOPAZ reanalysis  
 185 on the gyre index. Only significant values at 95 % level are shown. Contours are bottom topography drawn at every 1000 m.

186 To elucidate the possible influence of atmospheric circulation pattern associated with GSG circulation on the SIC variability  
 187 in the GS, linear regression of the sea level pressure anomalies on the gyre index was calculated and shown in Fig. 6. The  
 188 large-scale atmospheric circulation shows a positive NAO-like pattern associated with a strong GSG circulation, but with  
 189 centres of actions north of their usual locations (Fig. 6). The GSG circulation responds to the anomalous wind stress curl  
 190 induced by the low SLP anomaly patterns in the NS (Chatterjee et al. 2018). However, we found that the station based NAO  
 191 index, with its spatial feature highlighting the Icelandic low and Azores high,  
 192 ([https://climatedataguide.ucar.edu/sites/default/files/nao\\_station\\_seasonal.txt](https://climatedataguide.ucar.edu/sites/default/files/nao_station_seasonal.txt)) and the gyre index have a very low correlation  
 193 ( $r = 0.2$ ). This further points to the importance of the spatial variability of NAO (Zhang et al. 2008; Moore et al. 2012) and  
 194 its influence on the Nordic Seas circulation. Also note that the low correlation could be due to the fact that the equatorward  
 195 pole of NAO doesn't exhibit much significant regression patterns in Fig. 6.

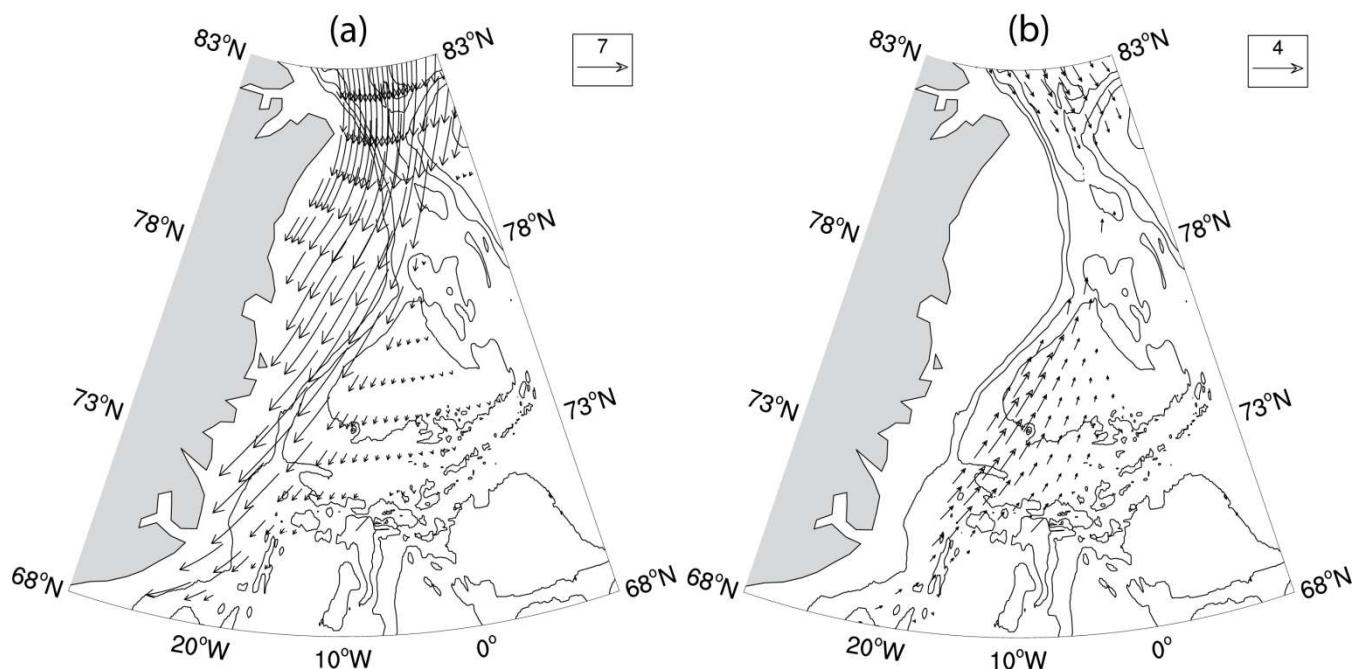


196

197 **Figure 6:** Linear regression of DJF mean sea level pressure anomaly on the gyre index. Regions with 95% statistical  
 198 significance are dotted.

199 The mean southward sea ice export in the GS across the FS (Fig 7a) is strongly driven by the geostrophic winds in this  
 200 region (Smedsrud et al. 2017). The low SLP pattern over NS associated with the GSG circulation can induce anomalous  
 201 northerlies in GS. Linear regression of sea ice velocities on the gyre index showed anomalous northward sea ice velocities in  
 202 GS associated with increase in GSG strength (Fig. 7b). This indicates that the anomalous northerly winds during a strong  
 203 GSG circulation would lead to Ekman drift of sea ice which tends to push the sea ice towards the Greenland coast and reduce

204 the mean southward sea ice velocities in this region (Fig. 7a). This could lead to reduced sea ice export in this region and  
205 result in low SIC.

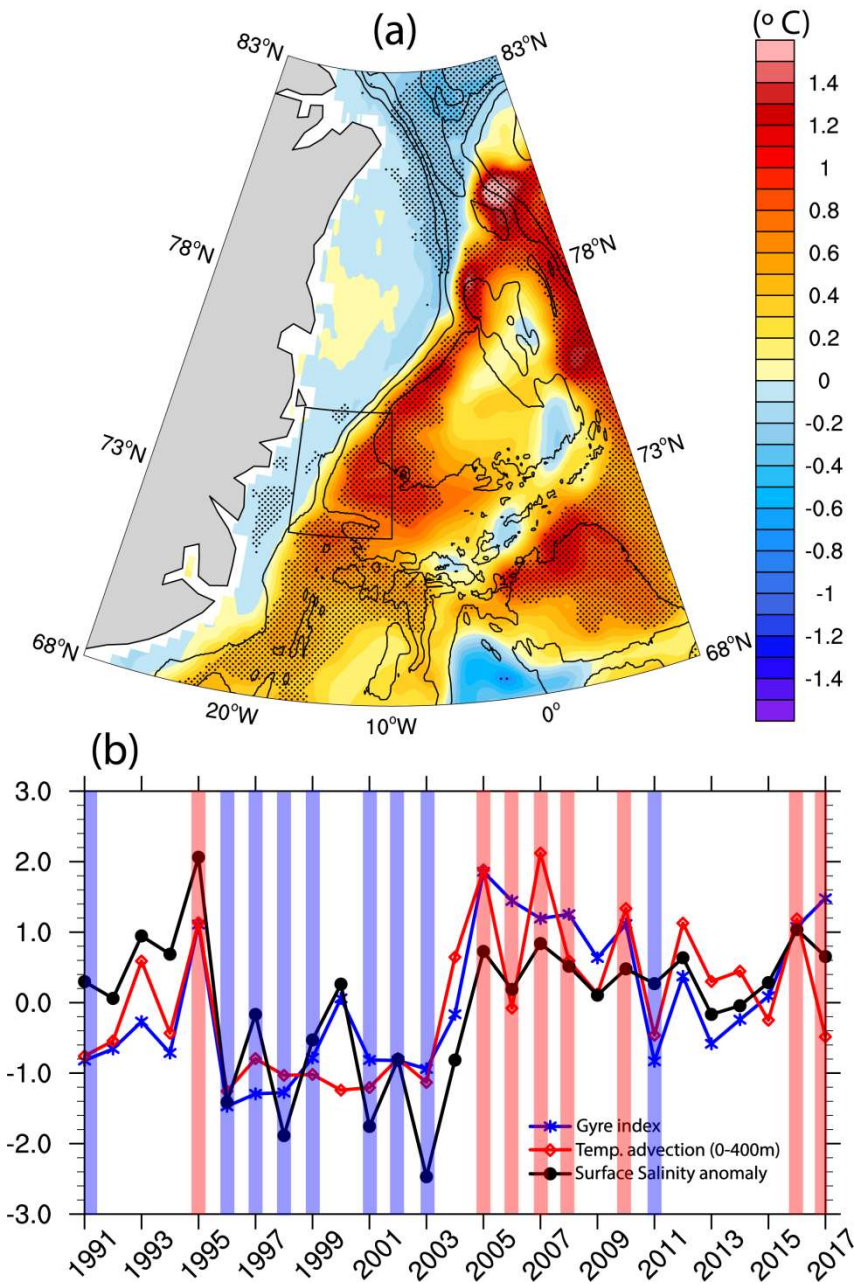


206

207

208 **Figure 7:** (a) Climatological (1991–2017) DJF sea ice velocity vectors (cm/s) from satellite observations. (b) Regression of  
209 DJF sea ice velocity anomalies (cm/s) on the gyre index. Only results significant at 95 % are shown for clarity. Contours are  
210 bottom topography drawn at every 1000 m.

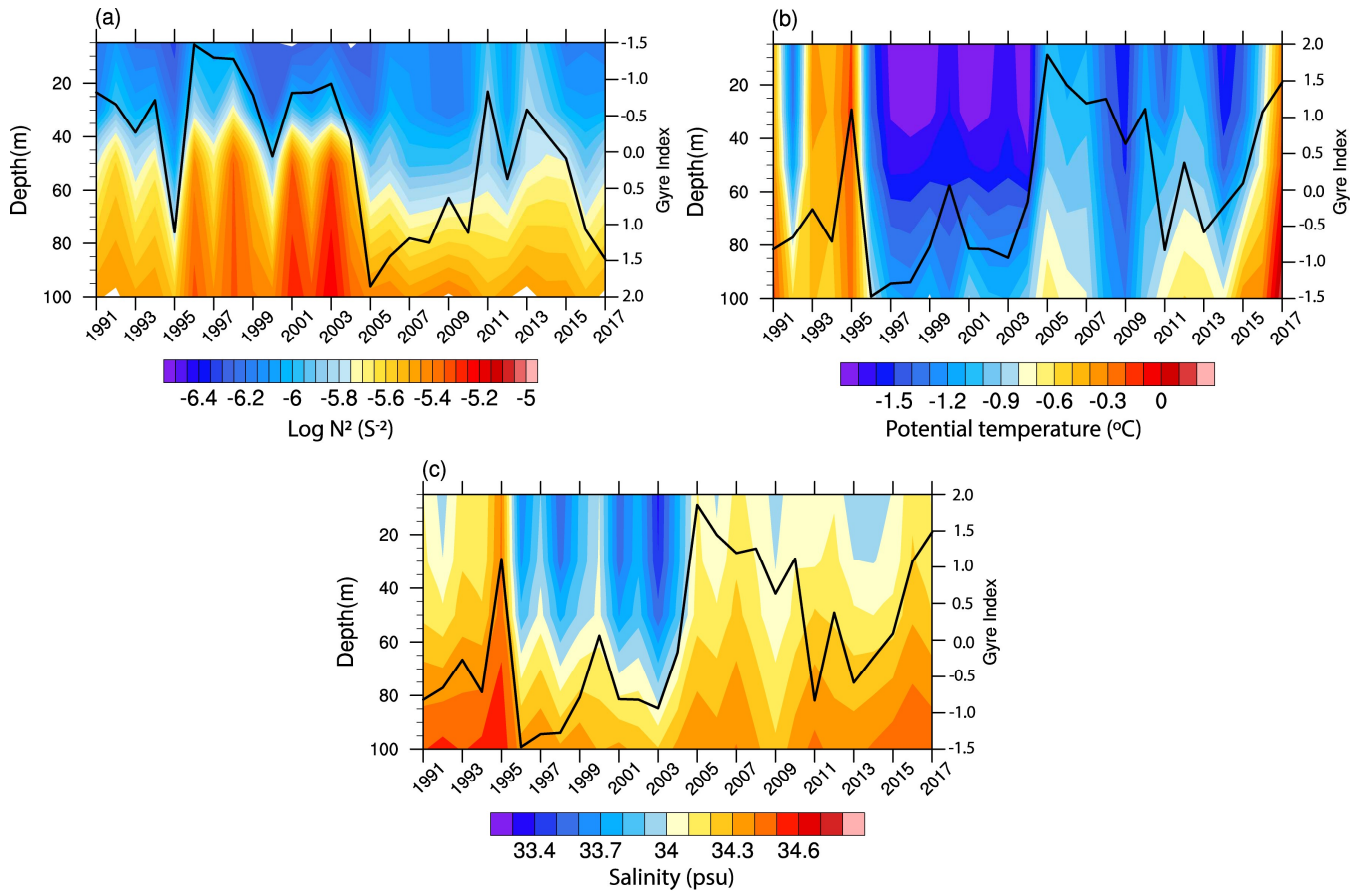
211 Next, we investigate GSG’s potential in influencing the oceanic conditions and hence the sea ice in the GS, given that the  
212 local oceanic conditions largely affect the sea ice conditions therein (Johannessen et al. 1987; Visbeck et al. 1995; Kern et al.  
213 2010; Selyuzhenok et al. 2020). Figure 8a shows the difference in ocean temperature anomaly in the upper 400m averaged  
214 for the strong and weak GSG circulation years (marked in Fig 8b; see methods for definitions). The average temperature  
215 anomaly for the strong GSG circulation years was found to be  $\sim 1^{\circ}\text{C}$  higher than the same during weak GSG circulation  
216 years. The warm anomalies further extend eastward with the JMC towards the central GS and could potentially affect the sea  
217 ice formation in the Odden region. Further, we found significant positive correlation ( $r=0.7$ ,  $p<0.01$ ; Fig 8b) between gyre  
218 index and temperature advection ( $U \cdot \nabla T$  in upper 400m) in the south-western GS (marked region in Fig. 8a), where  
219 maximum GSG influence on SIC is found (Fig. 3a). This suggests that a strong GSG circulation recirculates the warm AW  
220 anomalies into the south-western GS from the FS. This is consistent with earlier study indicating an increased oceanic heat  
221 content in the south-western GS due to a stronger GSG circulation (Chatterjee et al., 2018).



223

224 **Figure 8:** (a) Difference between 400 m depth averaged potential temperature anomalies (°C) averaged for strong (red bars  
 225 in (b)) and weak (blue bars in (b)) gyre index years. (b) Gyre index (blue), and standardized surface salinity anomaly (black),  
 226 temperature advection ( $U \cdot \nabla T$ ) in upper 400 m (red) for DJF over the region 72 N: 75 N; 18 W : 10 W, as marked in (a).

227 However, it should be noted that the recirculated AW in the GS still remains dense enough to be in subsurface (Schlichtholz  
 228 & Houssais 1999; Eldevik et al. 2009) and needs to be vertically mixed to have an impact on the sea ice. We found that the  
 229 upper ocean stratification in the south-western GS strongly covaries with GSG circulation strength (Fig. 9a). The analysis  
 230 shows that a weakening of the stratification in the upper part of the water column coincides with a stronger GSG circulation  
 231 and vice versa (Fig. 9a). Further, warm and saline signatures in the upper ocean can be found during strong GSG circulation,  
 232 indicating enhanced vertical mixing of the AW in the south-western GS (Figs. 9b,c). This is further confirmed by significant  
 233 positive correlation ( $r=0.7$ ,  $p<0.01$ ) between surface salinity anomaly and gyre index (Fig. 8b). These surface anomalies can  
 234 further inhibit new sea ice formation and also may cause melting of existing sea ice from the bottom.



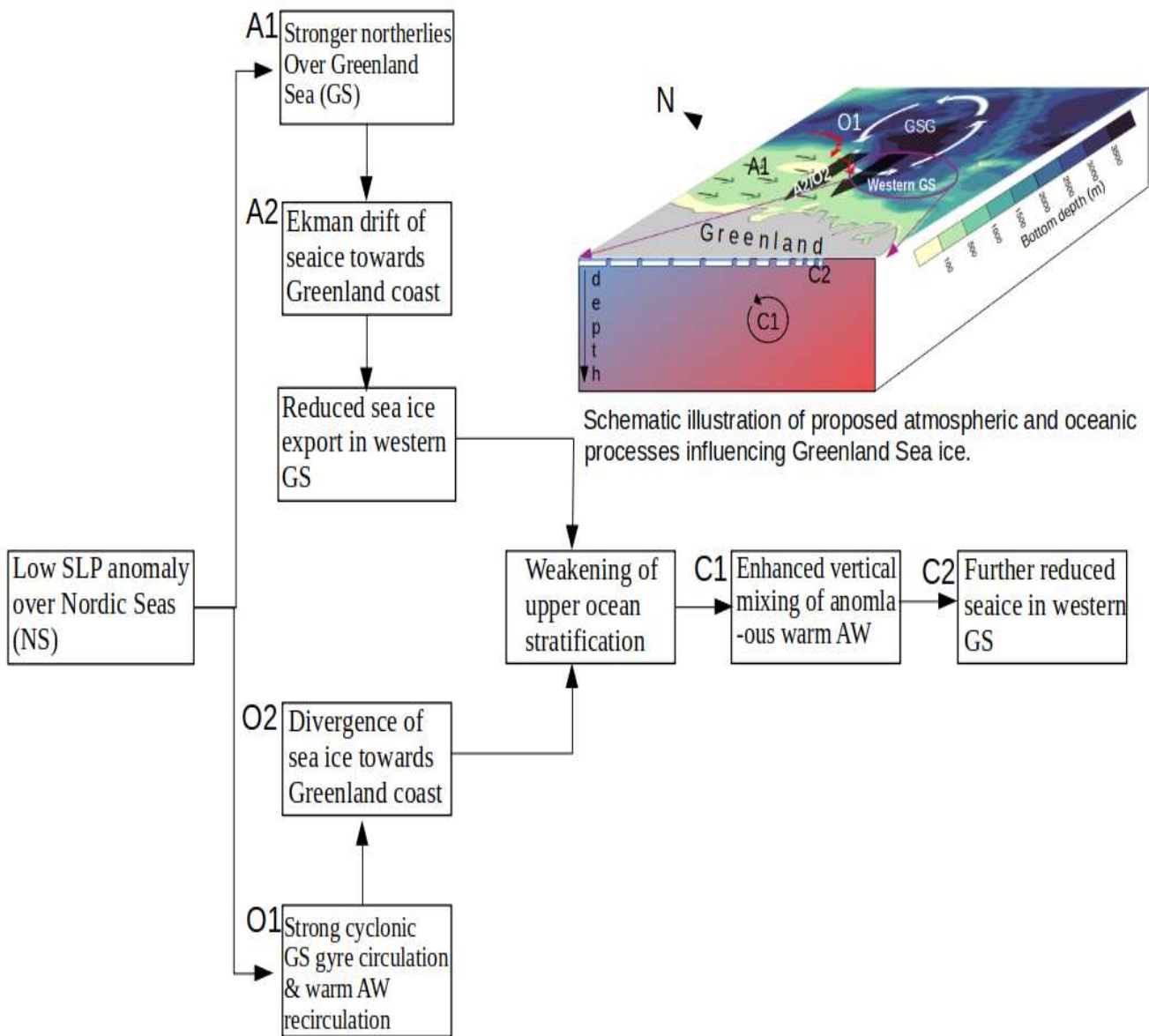
235

236

237 **Figure 9:** (a) Logarithm of squared Brunt-Väisälä Frequency ( $N^2$ , colour shaded) (b) potential temperature (c) salinity for  
 238 DJF over the region 72 N:75 N; 18 W:10 W, as marked in Figure 8a. The black timeseries against the right Y axis is the gyre  
 239 index in all three panels. Note that the gyre index is plotted against a reversed Y axis in (a) for ease of comparison.

#### 240 **4. Discussions and Conclusions**

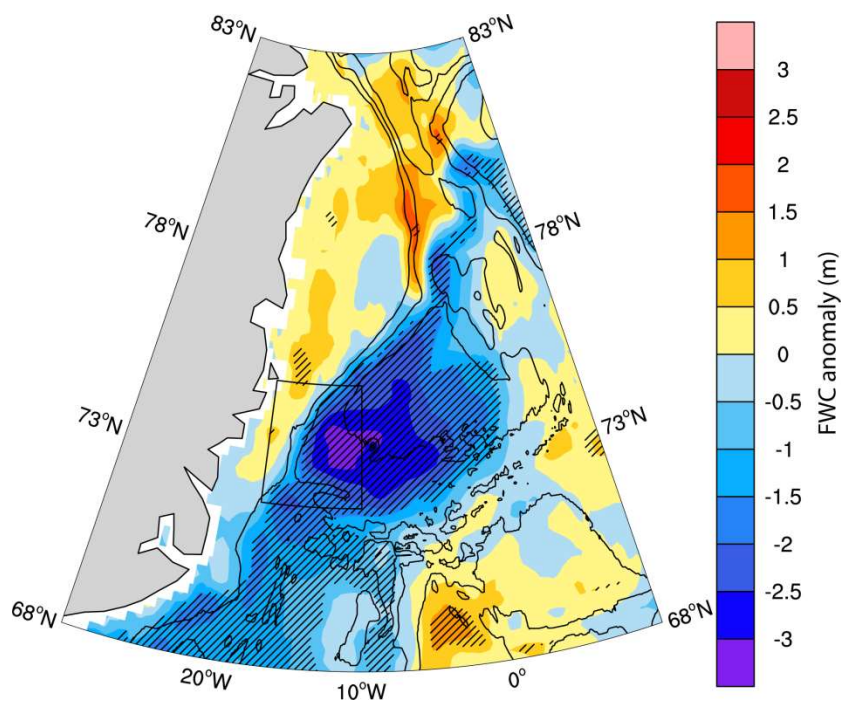
241 Here we investigated the combined influence of atmospheric and oceanic circulations on the interannual variability of the  
242 winter mean SIC variability in the GS and showed that NS, in particular the GSG circulation can significantly contribute to  
243 the SIC variability in south-western GS. Fig. 10 shows the flow chart and a schematic illustration of the mechanisms  
244 proposed in this study. The large-scale atmospheric circulation pattern that influences the GSG circulation resembles a  
245 NAO-like pattern with its northern centre of action situated northeast of the typical NAO pattern. The cyclonic GSG  
246 circulation strengthens in response to the positive wind stress curl induced by the low SLP anomaly in the NS (Legutke  
247 2002, Chatterjee et al. 2018). The resulting northerly wind anomalies over GS can potentially alter the sea ice export across  
248 the FS (Kwok & Rothrock 1999; Jung & Hilmer 2001; Vinje 2001; Tsukernik et al. 2010; Smedsrud et al. 2011; Ionita et al.  
249 2016). However, winter mean SIC in the GS and FS ice area flux are not strongly correlated (Kwok et al., 2004; Germe et  
250 al., 2011), suggesting that the SIC variability in the GS can be significantly influenced by the local sea ice dynamics and  
251 oceanic conditions.



252  
 253 **Figure 10:** A flow chart and schematic diagram of the proposed processes influencing the SIC variability in the south-  
 254 western GS.

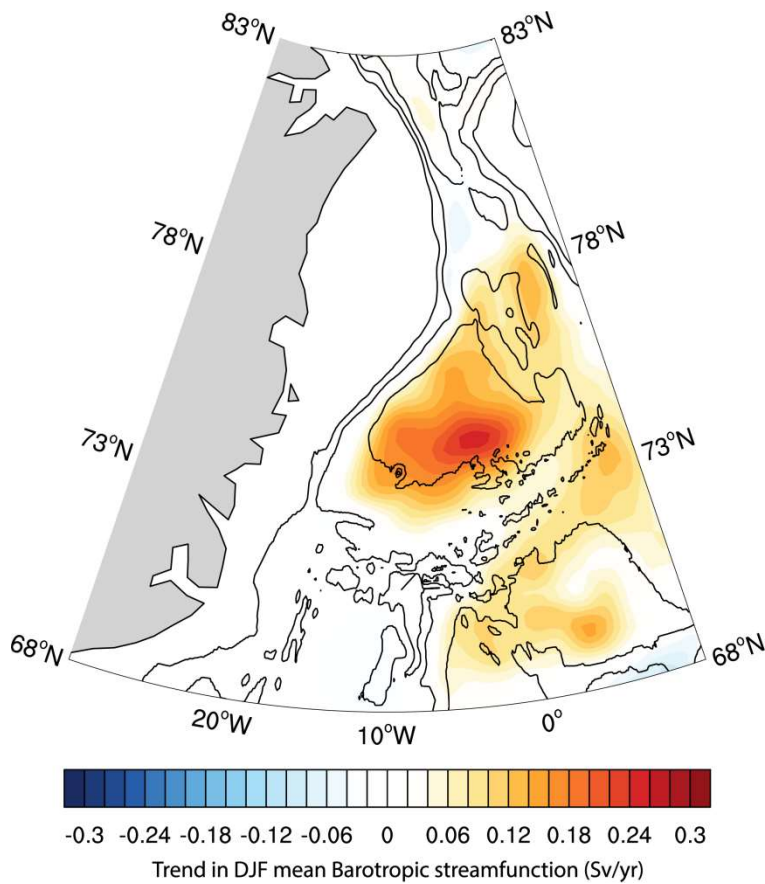
255  
 256 Anomalous winds in the Nordic Seas are known to influence the SIC in the GS through Ekman drift of the sea ice (Germe et  
 257 al., 2011). During time-periods with anomalously low SLP over NS, anomalous northerly winds and associated Ekman drift

258 towards the Greenland coast that can reduce the sea ice export in the western and central GS (Fig 8b). Enhanced Ekman  
 259 divergence due to a strengthened GSG circulation can further lead to reduced freshwater and sea ice in the south-western GS  
 260 (Fig. 11). We found that these can lead to weakening of the upper ocean stratification in the south-western GS (Fig. 9a). At  
 261 the same time, a stronger GSG circulation recirculates the warm and saline subsurface AW anomalies from the FS into the  
 262 south-western GS (Fig 8a). These AW anomalies can warm the surface waters by enhanced vertical mixing in a weakly  
 263 stratified condition (Fig. 9) and can cause further reduction of SIC by inhibiting new sea ice formation or even melting the  
 264 sea ice from bottom. Although our study doesn't show bottom melting of the sea ice, this can be realized from the findings  
 265 by Ivanova et al. (2011) which showed enhanced bottom melting in this region during positive NAO periods. Thus, the SIC  
 266 variability in the south-western GS responds to simultaneous influences from the atmospheric and oceanic circulation (Fig.  
 267 10). Despite the known influences of smaller scale processes, such as eddies and wave interactions on the SIC in the south-  
 268 western GS, our results show that the larger scale processes can also significantly affect the SIC variability in the region,  
 269 particularly on interannual timescales when the impacts of smaller scale processes can cancel out or may not be strong  
 270 enough to dampen the impact of larger scale processes. However, as found in Raj et al., (2020) interactions between the gyre  
 271 circulation and the eddies can be an important factor controlling the oceanic conditions and hence the SIC in the south-  
 272 western GS.



273  
 274 **Figure 11:** Difference in freshwater content (FWC) anomaly (m) between strong and weak gyre index periods. Significant  
 275 differences at 95% level are stippled.

276



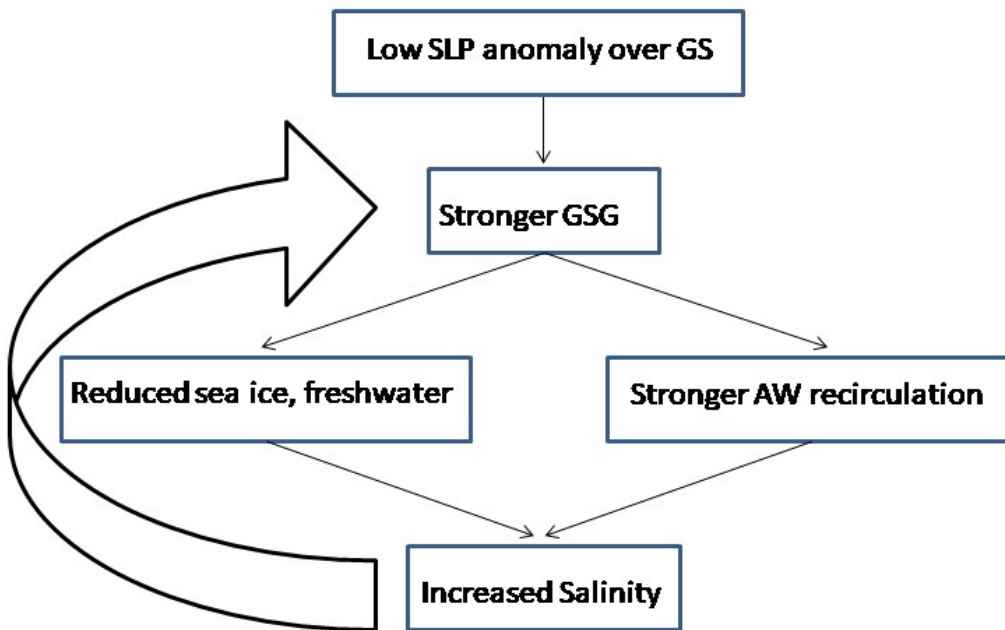
277  
278

279 **Figure 12:** Linear trend (Sv/year) in winter mean (DJF) barotropic stream function for 1991–2017. Only significant values at  
280 95 % level are shown for clarity. Contours are bottom topography drawn at every 1000 m.

281

282 This study finds one of the mechanisms of SIC variability in the GS, highlighting the role of large scale atmospheric and  
283 oceanic circulations in the NS. Observations and modelling results suggest stronger atmospheric forcing in the NS due to  
284 spatial variation of the NAO (Zhang et al. 2008) and its tendency towards positive phase in a warmer climate (Bader et al.  
285 2011; Stephenson et al. 2016). Consistent with that we find a significant positive trend in the GSG circulation strength  
286 during the study period (Fig. 12). The response of GSG circulation to this altered atmospheric forcing can further be realized  
287 with increased GSG strength (Fig. 1c) and a northeastward displacement of NAO's poleward centre of action in the Nordic  
288 Seas during early 2000s (Fig. 1a in Zhang et al., 2008). Recent observations further suggest intensified convection in the  
289 GSG and changes in water mass formation during the last two decades (Lauvset et al., 2018; Brakstad et al., 2019). Lauvset  
290 et al., (2018) further discussed the role of recirculated AW on inducing intensified convection in the GSG through surface  
291 salinity anomaly. Consistent with this, our results show that the salinity anomalies and intensified convection in the GSG can  
292 be induced by a stronger GSG circulation (in response to the atmospheric forcing) which helps in recirculation of AW

293 anomalies in the GS. Thus we propose that the atmospheric forcing over the NS imposes a positive oceanic feedback (Fig.  
294 13). The low SLP anomaly over the NS strengthens the GSG circulation. The Ekman divergence pushes the freshwater and  
295 sea ice from the GS interior towards the coast. Enhanced AW recirculation due to a stronger GSG and weakened  
296 stratification due to reduced freshwater allows the warm and saline AW anomalies to get vertically mixed and increase the  
297 temperature and salinity in the central GS. The increased salinity further helps in a stronger GSG circulation, completing the  
298 feedback loop. It should be noted that the complex subsurface processes and their interactions with the large scale circulation  
299 are often difficult to capture in the reanalysis, particularly with sporadic subsurface observations in both time and space. For  
300 example, while the surface variables are well captured in TOPAZ4, the reanalysis is too warm in the GS below 300 m as  
301 observed in Xie et. al, 2017 (their Figure 9). Of particular interest in this study, the south-western GS, is a particularly sparse  
302 region in observational data. Increased long-term observations from these areas would help improving the reanalysis datasets  
303 and better understand the complex atmosphere-ocean interactions and their impact on the sea ice variability of this region.



304

305 **Figure 13:** A proposed positive oceanic feedback induced by atmospheric forcing in NS.

306

307

308 **Acknowledgments**

309 Sea ice concentration (<https://nsidc.org/data/NSIDC-0051/versions/1>) and velocity (<https://nsidc.org/data/nsidc-0116/versions/4>) are obtained from the National Snow and Ice Data Centre. The TOPAZ4 simulations have used grants of computing time (nn2993k) and storage (ns2993k) from the Sigma2 infrastructure. The monthly TOPAZ4 results used in this study are obtained via CMEMS ([marine.copernicus.eu](http://marine.copernicus.eu)). EN4 (version 4.2.1) observational data is provided by UK Met Office Hadley Centre and obtained from <https://www.metoffice.gov.uk/hadobs/en4/download-en4-2-1.html>. Authors thank Ola M Johannessen, Nansen Scientific Society for valuable suggestions during the course of the study. All figures were made using The NCAR Command Language (Version 6.4.0).

316

317 **Declarations**

318 **Funding** (information that explains whether and by whom the research was supported)

319 Not Applicable

320 **Conflicts of interest/Competing interests** (include appropriate disclosures)

321 Authors declare no Conflicts of interest/Competing interests

322 **Availability of data and material** (data transparency)

323 All the data used here are freely available on respective data portals (links provided in the ‘Acknowledgements’ section)

324 **Code availability (software application or custom code)**

325 All the codes are available on reasonable request to the corresponding author.

326 **Authors' contributions**

327 SC conceived the idea in discussion with RPR and LB wrote the manuscript. SC performed all the analyses. All authors contributed in drafting and improvement of the manuscript.

329

330

331

332

333

334

335

336

337

338

339

340 **References**

- 341 Aagaard, K.: Wind-driven transports in the Greenland and Norwegian seas, *Deep. Res. Oceanogr. Abstr.*, doi:10.1016/0011-  
342 7471(70)90021-5, 1970.
- 343 Aagaard, K. and Carmack, E. C.: The role of sea ice and other fresh water in the Arctic circulation, *J. Geophys. Res.*,  
344 doi:10.1029/jc094ic10p14485, 1989.
- 345 Bader, J., Mesquita, M. D. S., Hodges, K. I., Keenlyside, N., Østerhus, S. and Miles, M.: A review on Northern Hemisphere  
346 sea-ice, storminess and the North Atlantic Oscillation: Observations and projected changes, *Atmos. Res.*,  
347 doi:10.1016/j.atmosres.2011.04.007, 2011.
- 348 Belkin, I. M., Levitus, S., Antonov, J. and Malmberg, S. A.: “Great Salinity Anomalies” in the North Atlantic, *Prog.*  
349 *Oceanogr.*, doi:10.1016/S0079-6611(98)00015-9, 1998.
- 350 Bourke, R. H., Paquette, R. G. and Blythe, R. F.: The Jan Mayen Current of the Greenland Sea, *J. Geophys. Res.*,  
351 doi:10.1029/92jc00150, 1992.
- 352 Brakstad, A., K. Våge, L. Håvik, and G. W. K. Moore, 2019: Water Mass Transformation in the Greenland Sea during the  
353 Period 1986–2016. *J. Phys. Oceanogr.*, 49, 121–140, <https://doi.org/10.1175/JPO-D-17-0273.1>.
- 354 Campbell, W. J., Gloersen, P., Josberger, E. G., Johannessen, O. M., Guest, P. S., Mognard, N., Shuchman, R., Burns, B. A.,  
355 Lannelongue, N. and Davidson, K. L.: Variations of mesoscale and large-scale sea ice morphology in the 1984 marginal ice  
356 zone experiment as observed by microwave remote sensing, *J. Geophys. Res. Ocean.*, doi:10.1029/JC092iC07p06805, 1987.
- 357 Cavalieri, D.J., Parkinson, C. L., Gloersen, P. & Zwally H. J.: Sea Ice Concentrations From Nimbus-7 SMMR and DMSP  
358 SSM/I Passive Microwave Data, *Natl. Snow and Ice Data Cent.*, Boulder, Colorado, 1996 [Updated 2018].
- 359 Chafik L., and Rossby T.: Volume, heat, and freshwater divergences in the Subpolar North Atlantic suggest the Nordic Seas  
360 as key to the state of the Meridional Overturning Circulation. *Geophysical Research Letters* 46: doi:10.1029/2019GL082  
361 110. 2019
- 362 Chatterjee, S., Raj, R. P., Bertino, L., Skagseth, Ravichandran, M. and Johannessen, O. M.: Role of Greenland Sea Gyre  
363 Circulation on Atlantic Water Temperature Variability in the Fram Strait, *Geophys. Res. Lett.*, doi:10.1029/2018GL079174,  
364 2018.
- 365 Comiso, J. C., Wadhams, P., Pedersen, L. T. and Gersten, R. A.: Seasonal and interannual variability of the Odden ice  
366 tongue and a study of environmental effects, *J. Geophys. Res. Ocean.*, doi:10.1029/2000jc000204, 2001.

367

368

369 Dee, D. P., Uppala, S. M., Simmons, A. J., Berrisford, P., Poli, P., Kobayashi, S., Andrae, U., Balmaseda, M. A., Balsamo,  
370 G., Bauer, P., Bechtold, P., Beljaars, A. C. M., van de Berg, L., Bidlot, J., Bormann, N., Delsol, C., Dragani, R., Fuentes, M.,  
371 Geer, A. J., Haimberger, L., Healy, S. B., Hersbach, H., Hólm, E. V., Isaksen, L., Kållberg, P., Köhler, M., Matricardi, M.,  
372 McNally, A. P., Monge-Sanz, B. M., Morcrette, J. J., Park, B. K., Peubey, C., de Rosnay, P., Tavolato, C., Thépaut, J. N. and  
373 Vitart, F.: The ERA-Interim reanalysis: Configuration and performance of the data assimilation system, *Q. J. R. Meteorol.*  
374 *Soc.*, doi:10.1002/qj.828, 2011.

375 Deser, C., Walsh, J. E. and Timlin, M. S.: Arctic sea ice variability in the context of recent atmospheric circulation trends, *J.*  
376 *Clim.*, doi:10.1175/1520-0442(2000)013<0617:ASIVIT>2.0.CO;2, 2000.

377 Dickson, R. R., Meincke, J., Malmberg, S. A. and Lee, A. J.: The “great salinity anomaly” in the Northern North Atlantic  
378 1968-1982, *Prog. Oceanogr.*, doi:10.1016/0079-6611(88)90049-3, 1988.

379 Eldevik, T., Nilsen, J. E., Iovino, D., Anders Olsson, K., Sandø, A. B. and Drange, H.: Observed sources and variability of  
380 Nordic seasovertflow, *Nat. Geosci.*, doi:10.1038/ngeo518, 2009.

381 Germe, A., Houssais, M. N., Herbaut, C. and Cassou, C.: Greenland Sea sea ice variability over 1979-2007 and its link to the  
382 surface atmosphere, *J. Geophys. Res. Ocean.*, 116(10), 1–14, doi:10.1029/2011JC006960, 2011.

383 Grebmeier, J. M., Smith, W. O. and Conover, R. J.: Biological processes on Arctic continental shelves: Ice-ocean-biotic  
384 interactions., 2011.

385 Hattermann, T., Isachsen, P. E., Von Appen, W. J., Albretsen, J. and Sundfjord, A.: Eddy-driven recirculation of Atlantic  
386 Water in Fram Strait, *Geophys. Res. Lett.*, doi:10.1002/2016GL068323, 2016.

387 Hilmer, M. and Jung, T.: Evidence for a recent change in the link between the North Atlantic Oscillation and Arctic sea ice  
388 export, *Geophys. Res. Lett.*, doi:10.1029/1999GL010944, 2000.

389 Huang, J., Pickart, R.S., Huang, R.X., Lin, P., Brakstad, A. and Xu, F.: Sources and upstream pathways of the densest  
390 overflow water in the Nordic Seas. *Nat Commun.*, <https://doi.org/10.1038/s41467-020-19050-y>, 2020.

391 Hunke, E. C. and Dukowicz, J. K.: An elastic-viscous-plastic model for sea ice dynamics, *J. Phys. Oceanogr.*, 27, 1849–  
392 1867, 1997.

393 Hurrell, J. W.: Decadal trends in the North Atlantic oscillation: Regional temperatures and precipitation, *Science (80-. )*,  
394 doi:10.1126/science.269.5224.676, 1995.

395 Instanes, A., Anisimov, O., Brigham, L., Goering, D., Khrustalev, L. N., Ladanyi, B., Larsen, J. O., Smith, O., Stevermer,  
396 A., Weatherhead, B. and Weller, G.: Infrastructure: buildings, support systems, and industrial facilities, in *Arctic Climate*  
397 *Impact Assessment.*, 2005.

398 Ionita, M., Scholz, P., Lohmann, G., Dima, M. and Prange, M.: Linkages between atmospheric blocking, sea ice export  
399 through Fram Strait and the Atlantic Meridional Overturning Circulation, *Sci. Rep.*, doi:10.1038/srep32881, 2016.

400 Jeansson, E., Olsen, A. and Jutterström, S.: Arctic Intermediate Water in the Nordic Seas, 1991–2009, *Deep. Res. Part I*  
401 *Oceanogr. Res. Pap.*, doi:10.1016/j.dsr.2017.08.013, 2017.

402 Johannessen, O. M., Johannessen, J. A., Svendsen, E., Shuchman, R. A., Campbell, W. J. and Josberger, E.: Ice-edge eddies  
403 in the Fram Strait marginal ice zone, *Science (80-. )*, doi:10.1126/science.236.4800.427, 1987.

404 Johannessen, O. M., Bengtsson, L., Miles, M. W., Kuzmina, S. I., Semenov, V. A., Alekseev, G. V., Nagurnyi, A. P.,  
405 Zakharov, V. F., Bobylev, L. P., Pettersson, L. H., Hasselmann, K. and Cattle, H. P.: Arctic climate change: Observed and  
406 modelled temperature and sea-ice variability, *Tellus, Ser. A Dyn. Meteorol. Oceanogr.*, doi:10.1111/j.1600-  
407 0870.2004.00060.x, 2004.

408 Jung, T. and Hilmer, M.: The link between the North Atlantic oscillation and Arctic sea ice export through Fram Strait, *J.*  
409 *Clim.*, doi:10.1175/1520-0442(2001)014<3932:TLBTNA>2.0.CO;2, 2001.

410 Kern, S., Kaleschke, L. and Spreen, G.: Climatology of the nordic (irminger, greenland, barents, kara and white/pechora)  
411 seas ice cover based on 85 GHz satellite microwave radiometry: 1992-2008, *Tellus, Ser. A Dyn. Meteorol. Oceanogr.*,  
412 doi:10.1111/j.1600-0870.2010.00457.x, 2010.

413 Killworth, P. D.: On “Chimney” Formations in the Ocean, *J. Phys. Oceanogr.*, doi:10.1175/1520-  
414 0485(1979)009<0531:ofito>2.0.co;2, 1979.

415 Kwok, R.: Fram Strait sea ice outflow, *J. Geophys. Res.*, 109(C1), C01009, doi:10.1029/2003JC001785, 2004.

416 Kwok, R. and Rothrock, D. A.: Variability of Fram Strait ice flux temperature 2 , -7 % of the area of the Arctic Ocean . The  
417 winter area flux ranges from a minimum to a maximum of October May 1995 is 1745 km from a low of 1375 km the 1990  
418 flux to a high of 2791 km The sea level pressu, *J. Geophys. Res.*, 104(1998), 5177–5189, 1999.

419 Kwok, R., Cunningham, G. F., Wensnahan, M., Rigor, I., Zwally, H. J. and Yi, D.: Thinning and volume loss of the Arctic  
420 Ocean sea ice cover: 2003-2008, *J. Geophys. Res. Ocean.*, doi:10.1029/2009JC005312, 2009.

421 Lauvset, S.K., Brakstad, A., Våge, K., Olsen, A., Jeansson, E., Mork, K.A.: Continued warming, salinification and  
422 oxygenation of the Greenland Sea gyre, *Tellus A*, 70 (1), pp.1-9, doi:10.1080/16000870.2018.1476434, 2018.

423 Legutke, S.: A Numerical Investigation of the Circulation In the Greenland and Norwegian Seas, *J. Phys. Oceanogr.*,  
424 doi:10.1175/1520-0485(1991)021<0118:aniotc>2.0.co;2, 2002.

425 Levitus et al.: Global ocean heat content 1955-2008 in light of recently revealed instrumentation problems. *Geophysical*  
426 *Research Letters*, 36, L07608. doi:<http://dx.doi.org/10.1029/2008GL037155>, 2009

427 Lien, V. S., Hjøllo, S. S., Skogen, M. D., Svendsen, E., Wehde, H., Bertino, L., Counillon, F., Chevallier, M. and Garric, G.:  
428 An assessment of the added value from data assimilation on modelled Nordic Seas hydrography and ocean transports, *Ocean*  
429 *Model.*, doi:10.1016/j.ocemod.2015.12.010, 2016.

430 Lind, S., Ingvaldsen, R. B. and Furevik, T.: Arctic warming hotspot in the northern Barents Sea linked to declining sea-ice  
431 import, *Nat. Clim. Chang.*, doi:10.1038/s41558-018-0205-y, 2018.

432 Marshall, J. and Schott, F.: Open-ocean convection: Observations, theory, and models, *Rev. Geophys.*,  
433 doi:10.1029/98RG02739, 1999.

434 Moore, G. W. K., Renfrew, I. A. and Pickart, R. S.: Multidecadal mobility of the north atlantic oscillation, *J. Clim.*,  
435 doi:10.1175/JCLI-D-12-00023.1, 2013.

436 Nansen, F.: *Blant Sel og Bjørn. Min første Ishavs-Ferd [With Seals and Bears: My First Journey to the Arctic Seas]*, Jacob  
437 Dybwads Forlag, Oslo, 285 pp, 1924.

438 Raj, R. P., Chatterjee, S., Bertino, L., Turiel, A. & Portabella, M.: The Arctic Front and its variability in the Norwegian Sea,  
439 *Ocean Sci.*, 15, 1729–1744, <https://doi.org/10.5194/os-15-1729-2019>, 2019.

440 Raj, R. P., Halo, I., Chatterjee, S., Belonenko, T., Bakhoday-Paskyabi, M., Bashmachnikov, I., Federov, A., Xie P. :  
441 Interaction between mesoscale eddies and the gyre circulation in the Lofoten Basin. *Journal of Geophysical Research:*  
442 *Oceans*, 125, e2020JC016102. <https://doi.org/10.1029/2020JC016102>, 2020.

443 Rogers, J. C., and Hung, M.-P. (2008), The Odden ice feature of the Greenland Sea and its association with atmospheric  
444 pressure, wind, and surface flux variability from reanalyses, *Geophys. Res. Lett.*, 35, L08504, doi:10.1029/2007GL032938.

445 Sakov, P., Counillon, F., Bertino, L., Lister, K. A., Oke, P. R. and Korabely, A.: TOPAZ4: An ocean-sea ice data  
446 assimilation system for the North Atlantic and Arctic, *Ocean Sci.*, doi:10.5194/os-8-633-2012, 2012.

447 Schott, F., Visbeck, M. and Fischer, J.: Observations of vertical currents and convection in the central Greenland Sea during  
448 the winter of 1988-1989, *J. Geophys. Res.*, doi:10.1029/93jc00658, 1993.

449 Selyuzhenok, V., Bashmachnikov, I., Ricker, R., Vesman, A. & Bobylev, L.: Sea ice volume variability and water  
450 temperature in the Greenland Sea, *The Cryosphere*, 14, 477–495, <https://doi.org/10.5194/tc-14-477-2020>, 2020.

451 Serreze, M. C., Barrett, A. P., Slater, A. G., Woodgate, R. A., Aagaard, K., Lammers, R. B., Steele, M., Moritz, R.,  
452 Meredith, M. and Lee, C. M.: The large-scale freshwater cycle of the Arctic, *J. Geophys. Res. Ocean.*,  
453 doi:10.1029/2005JC003424, 2006.

454

455 Shuchman, R. A., Josberger, E. G., Russel, C. A., Fischer, K. W., Johannessen, O. M., Johannessen, J. and Gloersen, P.:  
456 Greenland Sea Odden sea ice feature: Intra-annual and interannual variability, *J. Geophys. Res. Ocean.*,  
457 doi:10.1029/98jc00375, 1998.

458 Smedsrud, L. H., Sirevaag, A., Kloster, K., Sorteberg, A. and Sandven, S.: Recent wind driven high sea ice area export in the  
459 Fram Strait contributes to Arctic sea ice decline, *Cryosphere*, doi:10.5194/tc-5-821-2011, 2011.

460 Stephenson, D. B., Pavan, V., Collins, M., Junge, M. M. and Quadrelli, R.: North Atlantic Oscillation response to transient  
461 greenhouse gas forcing and the impact on European winter climate: A CMIP2 multi-model assessment, *Clim. Dyn.*,  
462 doi:10.1007/s00382-006-0140-x, 2006.

463 Toudal, L.: Ice extent in the Greenland Sea 1978-1995, *Deep. Res. Part II Top. Stud. Oceanogr.*, doi:10.1016/S0967-  
464 0645(99)00021-1, 1999.

465 Tschudi, M., Meier, W. N., Stewart, J. S., Fowler, C. & Maslanik, J.: Polar Pathfinder Daily 25 km EASE-Grid Sea Ice  
466 Motion Vectors, Version 4. Boulder, Colorado USA. NASA National Snow and Ice Data Center Distributed Active Archive  
467 Center. Doi: <https://doi.org/10.5067/INAWUWO7QH7B>. 2019. [Updated 2019]

468 Tsukernik, M., Deser, C., Alexander, M. and Tomas, R.: Atmospheric forcing of Fram Strait sea ice export: A closer look,  
469 *Clim. Dyn.*, 35(7), 1349–1360, doi:10.1007/s00382-009-0647-z, 2010.

470 Våge, K., Papritz, L., Håvik, L., Spall, M. A. and Moore, G. W. K.: Ocean convection linked to the recent ice edge retreat  
471 along east Greenland, *Nat. Commun.*, doi:10.1038/s41467-018-03468-6, 2018.

472 Vinje, T.: Fram Strait Ice Fluxes and Atmospheric Circulation: 1950-2000, *J. Clim.*, doi:10.1175/1520-  
473 0442(2001)014<3508:FSIFAA>2.0.CO;2, 2001.

474 Visbeck, M., Fischer, J. and Schott, F.: Preconditioning the Greenland Sea for deep convection: ice formation and ice drift, *J.*  
475 *Geophys. Res.*, doi:10.1029/95jc01611, 1995.

476 Wadhams, P. and Comiso, J. C.: Two modes of appearance of the Odden ice tongue in the Greenland Sea, *Geophys. Res.*  
477 *Lett.*, doi:10.1029/1999GL900502, 1999.

478 Wadhams, P., Comiso, J. C., Prussen, E., Wells, S., Brandon, M., Aldworth, E., Viehoff, T., Allegrino, R. and Crane, D. R.:  
479 The development of the Odden ice tongue in the Greenland Sea during winter 1993 from remote sensing and field  
480 observations, *J. Geophys. Res. C Ocean.*, 101(C8), 18213–18235, doi:10.1029/96JC01440, 1996.

481 Xie, J., Bertino, L., Knut, L. and Sakov, P.: Quality assessment of the TOPAZ4 reanalysis in the Arctic over the period  
482 1991-2013, *Ocean Sci.*, doi:10.5194/os-13-123-2017, 2017.

- 483 Zamani, B., Krumpen, T., Smedsrud, L. H. and Gerdes, R.: Fram Strait sea ice export affected by thinning: comparing high-  
484 resolution simulations and observations, *Clim. Dyn.*, doi:10.1007/s00382-019-04699-z, 2019.
- 485 Zhang, X., Sorteberg, A., Zhang, J., Gerdes, R. and Comiso, J. C.: Recent radical shifts of atmospheric circulations and rapid  
486 changes in Arctic climate system, *Geophys. Res. Lett.*, doi:10.1029/2008GL035607, 2008